IEEE Access
Multidisciplinary | Rapid Review | Open Access Journal

Received July 3, 2020, accepted July 29, 2020, date of publication August 10, 2020, date of current version August 21, 2020.

Digital Object Identifier 10.1109/ACCESS.2020.3015437

A Quadtree Beam-Segmenting Based Wide-Swath SAR Polar Format Algorithm

XIN NIE, LONG ZHUANG, AND SHIJIAN SHEN
Nanjing Research Institute of Electronics Technology, Nanjing 210039, China
Corresponding author: Xin Nie (13913863864@139.com)

ABSTRACT The Polar Format Algorithm (PFA) is the most suitable imaging algorithm for high-resolution and highly-squinted spotlight Synthetic Aperture Radar (SAR), but the approximation of planar wavefront in this algorithm limits the effective scene size of PFA. To meet the wide-swath requirement in modern SAR system, a quadtree beam-segmenting based PFA is proposed in this paper. The original full-beam echo signal is filtered recursively as a quadtree, generating multiple sub-beams. Each sub-beam only illuminates a small part of the total swath. As long as the sub-beam is narrow enough, standard PFA could be utilized to process the sub-beam data. Each sub-beam data will result in a fully focused sub-image. Finally, all fully focused sub-images are mosaicked to get a big image perfectly focused. This divide-and-conquer approach breaks the image size limit in traditional PFA, extensively enlarges the effective scene. The processing flows are derived in detail and the algorithm is validated by simulated and measured data. Via the experiments, it could be seen that when the scene size exceeds the PFA limit, there would be serious defocus in the image obtained by traditional PFA, and the defocus could be eliminated by our new approach.

INDEX TERMS High-resolution and highly-squinted synthetic aperture radar (SAR), polar format algorithm (PFA), quadtree beam-segmenting, sub-beam, wide-swath.

I. INTRODUCTION

Synthetic aperture radar (SAR) [1]–[3] is an active ground-imaging system based on coherent processing of multiple radar echoes acquired along the path of a moving platform under all weather conditions. Although much of the literature discounts non-broadside imaging as atypical, highly-squinted imagery is becoming more widely available. Many modern spotlight SAR systems are especially aiming at nonbroadside imaging with squint angles possible up to or beyond $\pm 45°$. Generally, squint angle greater than 40° is considered to be highly squinted in SAR [4].

In highly squinted SAR, the echo signal is heavily coupled between range and cross-range, and it brings much difficulty for the imaging. In order to guarantee the imaging quality, many algorithms of high accuracy have been investigated to accommodate the high squint angle [4]–[12]. However, the complex mathematics expressions and the resulting complexities limit the future applications of the algorithms.

Meanwhile, the polar format algorithm (PFA) is adept at highly-squinted spotlight SAR [13], [14], since PFA has the following advantages: (1) PFA compensates the data to the line of sight (LOS) direction, so it could easily correct the range migration in highly squinted SAR and it has the same focusing accuracy for any squint angle. Generally, it is adapted to any squint angle as long as the radar is not illuminating the blind area [2], i.e. it is adapted to any squint angle smaller than 85°. (2) The dechirp process of PFA in slow-time domain reduces the azimuth bandwidth to be related to the azimuth size.

However, the approximation of the planar wavefront limits the PFA effective imaging size, and PFA has an effective focus radius limitation under different resolution conditions. For present high-resolution SAR applications with the resolution of 0.1m at X-band, the actual imaging requirements at least spans up to or beyond 1 km$\times$1 km. Meanwhile the effective focusing radius of PFA is only about 100m, which is far from meeting the actual imaging requirements. In recent years, the methods to solve the problem that the effective radius of PFA is too small mainly include two kinds, one is based on overlapping subaperture [15] and the other is space-variant post-processing [16], [17]. These two kinds of methods not only have low computation efficiency and high complexity of processing, but also are not accurate enough

The associate editor coordinating the review of this manuscript and approving it for publication was Brian Ng.

since they only derive the residual phase error to the second order. As the resolution requirements constantly increases, the expanded imaging scene is still not enough and need to be enlarged further more.

Based on the idea of digital spotlighting preprocessing [18]–[20], an improved quadtree beam-segmenting based PFA is proposed. Actually, this algorithm includes two parts of recursive segmentation. One part is to segment the image recursively, and the other part is to segment the echo data recursively. This procedure is equivalent to generate multiple sub-beam raw data. As long as each sub-beam is filtered narrow enough, standard PFA could be implemented to process the sub-beam data to produce a number of fully focused sub-images. Finally, all fully focused sub-images are stitched together to get a big image perfectly focused. This divide-and-conquer approach breaks the image size limit in traditional PFA, extensively enlarges the effective focused scene. Since this method is not based on the formula derivation of residual error, it is not restricted by the derivation order and can theoretically be extended to handle scene arbitrary large.

The idea of using beam segmentation scheme to overcome the PFA radius limitation problem sounds fairly simple, and the key point is how to maintain the reflected energy from each point target lossless and keep the desired resolution not degrading during the sub-beam segmentation. Moreover, we must consider how to keep the computation burden and the complexity of processing not increasing too much.

For these aspects, this paper is organized as follows. In Section II, the imaging geometry of squinted SAR is established, and the signal model of PFA is presented. The effect of the ''planar wavefront'' approximation in PFA and its size limitation is illustrated. In section III, the quadtree beam-segmenting based PFA is derived and presented in detail. In Section IV, the effectiveness of the proposed imaging method is demonstrated via simulation and real data experiments. The conclusion and further discussion are in Section V.

II. GEOMETRY AND ACCURATE SLANT RANGE MODEL

A. GEOMETRY OF SQUINTED SPOTLIGHT SAR

The classical squinted spotlight SAR imaging geometry is illustrated in Fig. 1, where the SAR sensor traveling at a fixed velocity v transmits a series of chirps to illuminate the ground target area. The scene center point $\boldsymbol{O}$ is defined as the origin, and the $\boldsymbol{O}$-xyz coordinate frame of the ground imaging area is shown in the figure, with y along the flight path, x perpendicular to the flight path, and z directs up to sky. The synthetic aperture is from A_{start} to A_{end}, with the aperture center A_c.

The line of sight (LOS) direction at aperture center is projected on the ground signed as x'-axis. The squint angle θ_0 is the rotation angle from (x, y) to (x', y') coordinate system. At instantaneous slow time t (in azimuth), $\phi = \phi(t), \theta = \theta(t)$ represent the instantaneous grazing angle and squint angle (the angle between the instantaneous LOS projection on ground and x-axis), respectively. And the angle between the instantaneous LOS projection on ground and x'-axis is $\hat{\theta}(t) = \theta(t) - \theta_0$. A_m represents an arbitrary radar position at time t. The instantaneous slant range between radar and the scene center is $r_a = r_a(t)$, and instantaneous slant range between radar and point target $P(x_p, y_p)$ is $r_p = r_p(t)$.

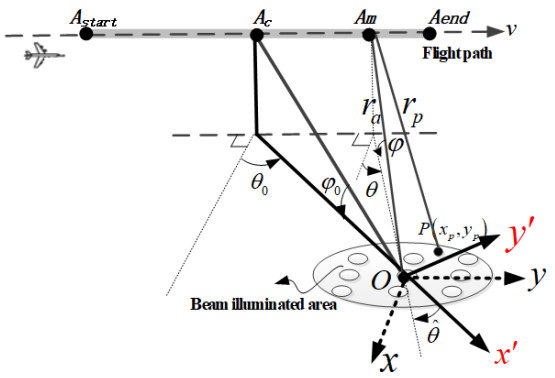

FIGURE 1. Highly squinted SAR geometry model.

B. ACCURATE SIGNAL MODEL AND PFA SIZE LIMIATION DUE TO PLANAR WAVEFRONT APPROXIMATION

According to the general geometry in Fig.1, assume that linear frequency modulated signal is transmitted, then the demodulated echoes can be expressed as

$$\begin{aligned} &s_1(t,\tau) \\ &= \iint_{(x_p,y_p)\in I} g(x_p,y_p)\cdot \mathrm{rect}\left(\frac{t-t_c}{T_a}\right)\cdot \mathrm{rect}\left(\frac{\tau-2r_p/c}{T_p}\right) \\ &\quad \cdot \exp\left[j\pi\gamma\left(\tau-2r_p/c\right)^2\right]\cdot \exp\left(-j\frac{4\pi f_c}{c}r_p\right)dx_p dy_p \end{aligned} \quad (1)$$

where $\boldsymbol{I}$ represents the ground illuminated area, rect$(\cdot)$ is a rectangular window, t is the azimuth time centered at $t_c = x_c/v$, T_a is the aperture time, τ is the range time, T_p is the pulse duration, c is the speed of light, f_c is centre frequency, γ is the chirp rate, and $g(x_p, y_p)$ represents the reflectivity of point target $P(x_p, y_p)$.

In the case of large squint angle and high resolution, the aperture time may be very long, and the range migration may be very severe, sometimes may extend to more than 10000m.

In the pre-process of PFA, it is common practice to implement Fast Fourier Transform (FFT) operation to transform the signal into range frequency domain as follows

$$\begin{aligned} &S_1(t,f_\tau) \\ &= \iint_{(x_p,y_p)\in I} g(x_p,y_p)\cdot \mathrm{rect}\left(\frac{t-t_c}{T_a}\right)\cdot \mathrm{rect}\left(\frac{f_\tau}{B_r}\right) \\ &\quad \cdot \exp\left(-j\pi\frac{f_\tau^2}{\gamma}\right)\cdot \exp\left[-j\frac{4\pi}{c}\left(f_c+f_\tau\right)r_p(t)\right]dx_p dy_p \end{aligned} \quad (2)$$

in which f_τ is the fast time frequency, i.e. range frequency.

Next step is to do the frequency domain match filtering and the 1st order motion compensation pulse by pulse. The scene center point is commonly chosen as the reference point of motion compensation, so this step is implemented by multiplying the conjugate of a hypothetical scene center echo in the range frequency domain as reference

$$S_I(t,f_\tau) = S_1(t,f_\tau)\cdot S_{ref}(t,f_\tau) \tag{3}$$

where

$$S_{ref}(t,f_\tau) = \mathrm{rect}\left(\frac{t-t_c}{T_a}\right)\cdot \mathrm{rect}\left(\frac{f_\tau}{B_r}\right) \cdot \exp\left(j\pi\frac{f_\tau^2}{\gamma}\right)\cdot \exp\left[j\frac{4\pi}{c}(f_c+f_\tau)\,r_a(t)\right] \tag{4}$$

After this 1st order motion compensation, the signal prepared for polar format storage is as follows:

$$S_I(t,f_\tau) = \int\limits_{(x_p,y_p)\in I} g(x_p,y_p)\cdot \mathrm{rect}\left(\frac{t-t_c}{T_a}\right)\cdot \mathrm{rect}\left(\frac{f_\tau}{B_r}\right) \cdot \exp\left\{j\frac{4\pi}{c}(f_c+f_\tau)\left[r_a(t)-r_p(t)\right]\right\}dx_p dy_p \tag{5}$$

Based on the Taylor series expansion, the differential range of $r_a(t)-r_p(t)$ could be expressed as

$$\begin{aligned} R_\Delta &= r_a(t)-r_p(t) \\ &= \frac{\vec{r}_p\cdot\vec{r}_a}{r_a} - \frac{r_p^2}{2r_a} + \frac{\left(\vec{r}_p\cdot\vec{r}_a\right)^2}{2r_a^3} + \frac{\left(\vec{r}_p\cdot\vec{r}_a\right)r_p^2}{2r_a^3} + \cdots \end{aligned} \tag{6}$$

where $\vec{r}_p = (x_p, y_p, z_p)$ is the target vector from scene center to point P, and $\vec{r}_a = (x_a, y_a, z_a)$ is the slant range vector from scene center to antenna phase center (APC). When the scene is small enough, the higher order term of the differential range above could be ignored, while only the first term is remained. This means that the wavefront is assumed planar. Under this approximation, the simplified differential distance can be expanded as

$$R_\Delta \approx \frac{\vec{r}_p\cdot\vec{r}_a}{r_a} = \hat{x}_\mathrm{p}\cos\phi\cos\hat{\theta} + \hat{y}_\mathrm{p}\cos\phi\sin\hat{\theta} \tag{7}$$

Azimuth time t is implicit in the angle $\phi = \phi(t), \theta = \theta(t)$, and $(\hat{x}_\mathrm{p}, \hat{y}_\mathrm{p})$ represents the coordinates of point $\boldsymbol{P}$ in the (x', y') coordinate system.

Apparently, the effective PFA imaging scene could not be too large. The allowable scene radius r_0 is decided by the carrier wavelength λ_c, the resolution requirement ρ_a and the imaging range R_{ac}, and the relation formula could be expressed as

$$r_0 \le \frac{2\rho_a}{K_a}\sqrt{\frac{R_{ac}}{\lambda_c}} \tag{8}$$

where K_a is the main lobe widening factor (generally let it be 1.3) [2].

III. A QUADTREE BEAM-SEGMENTING BASED PFA DESIGNED FOR WIDE-SWATH

As the required imaging scene gets larger and larger for present SAR systems, no matter in spotlight or sliding spotlight mode, the PFA residual error brought by planar wavefront approximation cannot be ignored. For a large scene, after PFA imaging, the central part of the scene (within the radius r_0) is non-defocus, while the outer part beyond the radius r_0 is defocused.

Our technique is to break wide beam into many sub-beams, it means breaking the large scene into many small pieces of limited size. If each piece of sub-scene is within the effective imaging scene radius r_0, no defocus will appear.

In order to make full use of the signal support area, traditional PFA commonly utilizes line-of-sight polar interpolation(LOSPI) [2] rather than stabilized scene polar interpolation (SSPI) to yield an image in which the scene orientation matches the squint angle, i.e. the PFA image will be in the (x', y') direction, with azimuth along y', and range along x'. Since the scene center point is chosen as the motion compensation point (MCP), the scene center will be the center of the resulting PFA image. Actually, what we need is only a hypothetical point as a reference point. So if we want to change the image center, we could choose another reference point to do the motion re-compensation. Use this digital processing method, the beam could be diverted to point at any direction artificially. This could be considered as digital beam-rotating.

Based on this idea, a quadtree beam-segmenting based PFA is proposed in this paper. In the first step, the original whole beam (corresponding to the whole imaging scene) data is decomposed into 4 narrow sub-beam data, each of which corresponds to a quadrant. That is the level-1 segmentation step shown in Fig. 2. And recursively, each set of the 4 sub-beam data is again decomposed into 4 narrower sub-beam data by level-2 segmentation, achieving 16 narrower sub-beam data after level-2 segmentation, as shown in Fig.2. In this way, the beam is recursively segmented one level by one level, like a Quadtree. The recursive beam segmentation could be stopped as long as each sub-scene is within the effective imaging scene radius r_0.

Firstly, we detail the first level of segmentation as below.

A. LEVEL-1 SEGMENTATION

The total imaged scene could be divided into 4 sub-scenes, by the reference axes in a Cartesian coordinate system, designated first, second, third, and fourth quadrant, counting counterclockwise from the area in which both coordinates are positive. In this step, we decompose the whole beam into 4 sub-beams based on the quadrant.

The specific process of one level of segmentation includes the following 4 steps:

1) CALCULATE THE CENTER COORDINATE OF 4 QUADRANTS

To rotate the beam direction pointing at each quadrant center, 4 reference points need to be chosen newly. Since $\boldsymbol{I}$ represents

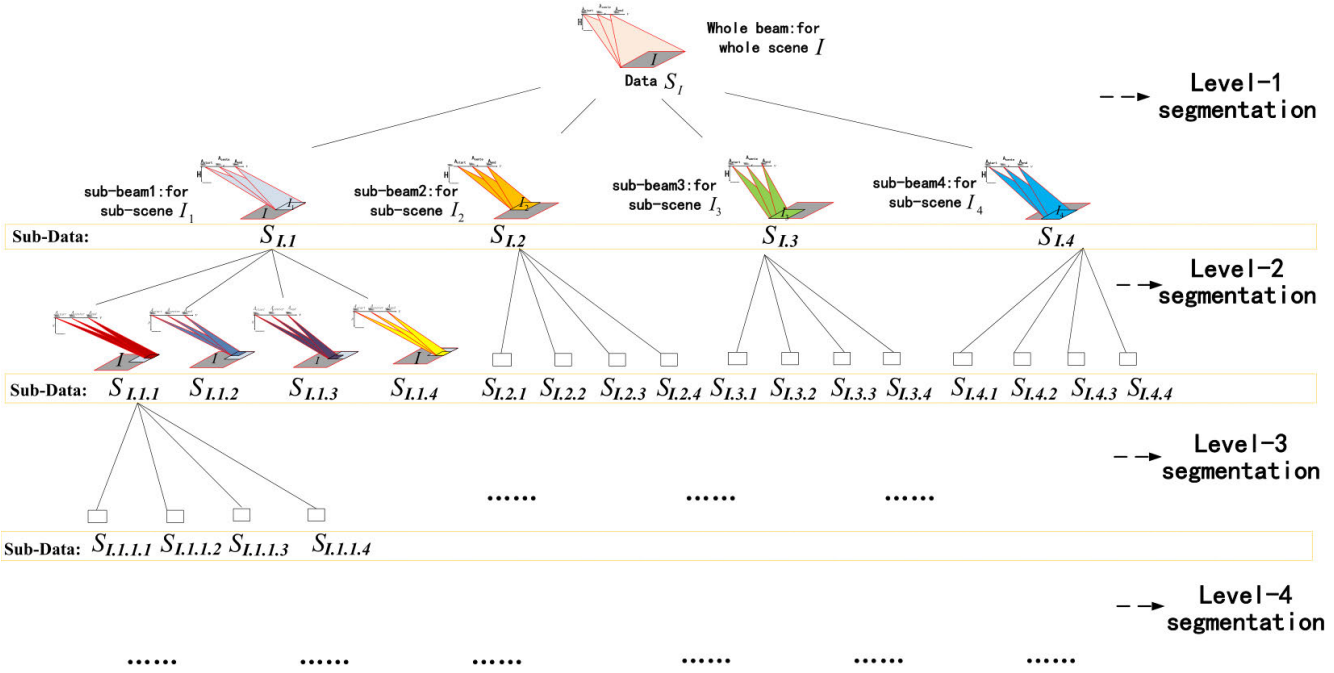

FIGURE 2. Recursive decomposition of beam and data as a Quadtree.

the ground illuminated area, here let $\boldsymbol{I.n}$ $(n = 1, 2, 3, 4)$, $C_{I.n}\left(x_{cI.n}, y_{cI.n}, z_{cI.n}\right)$ represent the each quadrant sub-scene and its sub-scene center point, respectively.

As long as the original azimuth size W_a (along y') and range size W_r (along x') of the illuminated scene can be calculated, the coordinates of each quadrant center could be calculated easily.

Taking 1st quadrant as an example, i.e. sub-scene $\boldsymbol{I.1}$ in Fig.2, its center point $C_{I.1}$ has the coordinates of

$$\begin{cases} x_{cI.1} = W_r/2 \cdot \cos\theta_0 + W_a/2 \cdot \sin\theta_0 \\ y_{cI.1} = -W_r/2 \cdot \sin\theta_0 + W_a/2 \cdot \cos\theta_0 \\ z_{cI.1} = 0 \end{cases} \tag{9}$$

2) MOTION RE-COMPENSATION TO EACH QUADRANT CENTER

In order to avoid energy leakage caused by defocusing, motion re-compensation is firstly needed for the original data. For each quadrant, the motion re-compensation function is constructed based on the central point, and the echo data is compensated pulse by pulse.

For the nth $(n = 1, 2, 3, 4)$ quadrant, the re-compensation phase is:

$$\varphi_{recom-I.n}(t, f_\tau) = \exp\left\{j\frac{4\pi}{c}(f_\tau + f_c)(r_{sI.n} - r_a)\right\} \tag{10}$$

where $r_{sI.n} = r_{sI.n}(t)$ is the instantaneous distance between the APC to $C_{I.n}$. And the re-compensated data is:

$$\begin{aligned} &S_{recom-I.n}(t, f_\tau) \\ &= \int\int_{(x_p, y_p)\in I} g(x_p, y_p) \cdot \mathrm{rect}\left(\frac{t - t_c}{T_a}\right) \cdot \mathrm{rect}\left(\frac{f_\tau}{B_r}\right) \\ &\quad \cdot \exp\left\{j\frac{4\pi}{c}(f_c + f_\tau)\left[r_{sI.n}(t) - r_p(t)\right]\right\} dx_p dy_p \end{aligned} \tag{11}$$

This echo still contains the whole scene information, but the beam is digital rotated to a new direction pointing at nth quadrant center.

Taking the 1st quadrant as an example, i.e. sub-image $\boldsymbol{I.1}$ in Fig.2, the re-compensation phase is:

$$\varphi_{recom-I.1}(t, f_\tau) = \exp\left\{j\frac{4\pi}{c}(f_\tau + f_c)(r_{sI.1} - r_a)\right\} \tag{12}$$

swhere $r_{sI.1} = r_{sI.1}(t)$ is the instantaneous distance between the APC to $C_{I.1}\left(x_{cI.1}, y_{cI.1}, z_{cI.1}\right)$, and it can be described in coordinates:

$$r_{sI.1} = \sqrt{(x_a - x_{cI.1})^2 + (y_a - y_{cI.1})^2 + z_a^2} \tag{13}$$

The new phase history after re-compensated to $C_{I.1}$ $\left(x_{cI.1}, y_{cI.1}, z_{cI.1}\right)$ is:

$$\begin{aligned} &S_{recom-I.1}(t, f_\tau) \\ &= \int\int_{(x_p, y_p)\in I} g(x_p, y_p) \cdot \mathrm{rect}\left(\frac{t - t_c}{T_a}\right) \cdot \mathrm{rect}\left(\frac{f_\tau}{B_r}\right) \\ &\quad \cdot \exp\left\{j\frac{4\pi}{c}(f_c + f_\tau)\left[r_{sI.1}(t) - r_p(t)\right]\right\} dx_p dy_p \end{aligned} \tag{14}$$

3) LINEAR RANGE DOPPLER (LRD) COARSE IMAGING AND CENTER SUB-IMAGE INTERCEPTED

Notice that last motion re-compensation step is actually equivalent to accomplish two-dimension dechirp to the original echo, eliminating the second order phase term of the signal. The azimuth and range frequency of each scatterer's two dimensional signal is proportional to scatterer distance from sub-scene center.

Suppose the re-compensationed data array size is $N \times N$, and a coarse focused image of size $N \times N$ can be obtained via a 2-dimesional (2-D) FFT. That is just the basic Linear Range Doppler (LRD [21]) algorithm. However, the center of the coarse focused image has been transferred to the center of each quadrant, and it means the useless information of other quadrants will be folded relative to the original image. Therefore, it is convenient to intercept the central part from the full image according to the subscripts. The array size after interception is $N/2 \times N/2$.

Taking 1st quadrant as an example, after motion re-compensation to $C_{I.1}$, the coarse focused LRD image is just centered at point $C_{I.1}$. What we need is that the sub-beam 1 only contains sub-scene I.1 information, and throwing away other unwanted information is easy in this coarse focused image.

After 4 quadrants are processed one by one, 4 coarse focused LRD sub-images could be achieved.

4) RETURNING TO THE PHASE HISTORY DOMAIN

Profiting from the dechirp, if the scene decreases, the bandwidth in azimuth and range domain corresponding to the phase history will be reduced as well. Accordingly, the sampling rate can be reduced in both azimuth and range, leading to a reduction of the computation.

The sub-image scene size is reduced to half in both range and azimuth dimension, so the sampling rate can be also reduced to half in both dimension. After returning the image to the spatial-frequency domain through Inverse Fast Fourier Transform (IFFT), the amount of data is reduced to the 1/4 of original, only containing the information of sub-scene ***I.1***. It is equivalent that the radar only uses a narrow-beam illuminates the sub-scene ***I.1*** area.

The sub-data for 1st quadrant after level-1 beam segmentation is represented as $S_{I.1}$, i.e. the sub-beam signal:

$$S_{I.1}(t, f_\tau) = \int\int_{(x_p, y_p) \in I.1} g(x_p, y_p) \cdot \mathrm{rect}\left(\frac{t - t_c}{T_a}\right) \cdot \mathrm{rect}\left(\frac{f_\tau}{B_r}\right) \cdot \exp\left\{j\frac{4\pi}{c}(f_c + f_\tau)\left[r_{sI.1}(t) - r_p(t)\right]\right\} dx_p dy_p \quad (15)$$

Here the sampling interval is doubled as much as that of the original. In summary, this process could be regarded as a fast filtering process, accomplishing information filter and down-sample at the same time. This operation is the key to keep the processing computation not increasing too much while maintaining the reflected energy from each point target lossless at the same time.

After 4 quadrants are processed one by one, 4 sub-data sets could be achieved. As Fig.2 shows, after level-1 segmentation, the original whole-beam echo data S_I is segmented into 4 sets of narrow sub-beam data. The nth($n = 1, 2, 3, 4$) sub-data is named by $S_{I.n}$, which only contains the nth quadrant (sub-image ***I.n***) information. The nth ($n = 1, 2, 3, 4$) output sub-beam data is represented as:

$$S_{I.n}(t, f_\tau) = \int\int_{(x_p, y_p) \in I.n} g(x_p, y_p) \cdot \mathrm{rect}\left(\frac{t - t_c}{T_a}\right) \cdot \mathrm{rect}\left(\frac{f_\tau}{B_r}\right) \cdot \exp\left\{j\frac{4\pi}{c}(f_c + f_\tau)\left[r_{sI.n}(t) - r_p(t)\right]\right\} dx_p dy_p \quad (16)$$

The flowchart of the 1st beam segmentation is illustrated in Fig.3. The key part to throw the unwanted information and implement the beam segmentation can be called Fast Filtering. The schematic diagram is shown in Fig. 4.

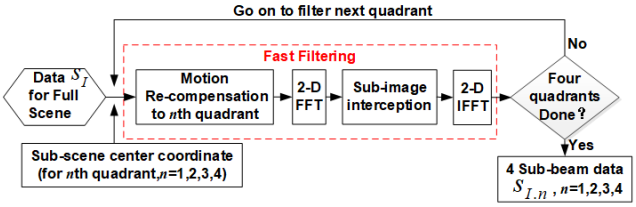

FIGURE 3. Flow diagram of 1st level of beam segmentation.

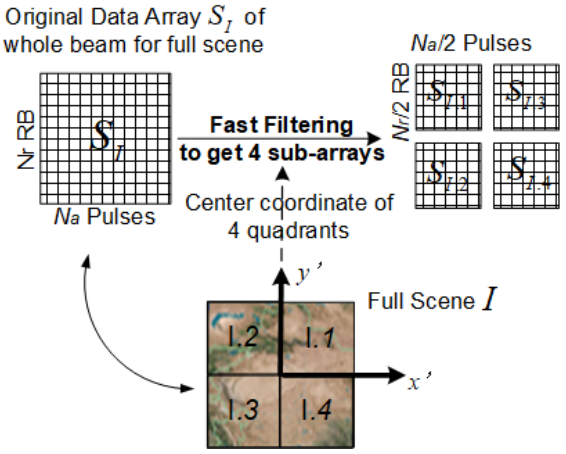

FIGURE 4. Schematic diagram of level-1 segmentation.

B. RECURSIVE BEAM SEGMENTATION AS A QUADTREE

After level-1 segmentation, the output sub-beam may be still too wide, since the corresponding sub-scene size may be still larger than the effective focusing scene size r_0. Therefore, it is necessary to segment the beam further, in order to ensure that the sub-scene illuminated by the segmented sub-beam is small enough, as shown in Fig.2 like a quadtree.

The naming principle of sub-scene and sub-beam data is shown in Fig.2, based on the Quadtree principle, beginning

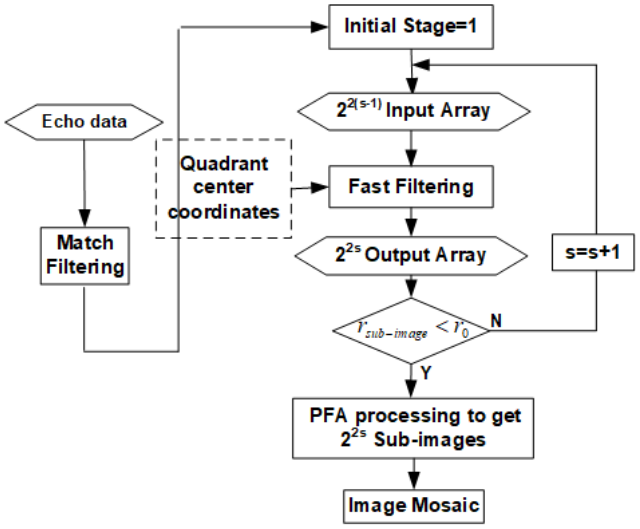

FIGURE 5. Flowchart of Quadtree beam-segmenting based PFA.

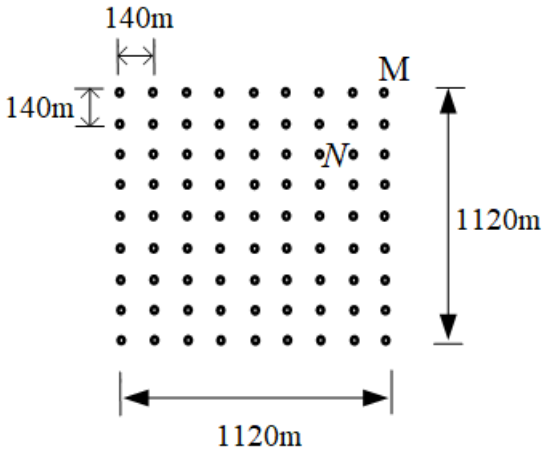

FIGURE 6. Simulated scene of point targets.

with $\boldsymbol{I}$, using its parent ID (identification) and the quadrant number.

Suppose the decomposition includes S level of quadtree segmentation, then for level-s (s= $1, 2 \ldots\ldots$ S) segmentation, there would be $2^{2(s-1)}$ set of input data, and 2^{2s} set of output data. The flow diagram of the proposed PFA is shown in Fig.5, where S represents the recursive decomposition level.

For each set of input echo data, the illuminated scene size and scene center needs to be calculated first. Then 4 quadrant center's position could be calculated easily, which will be used in motion re-compensation in fast filtering.

After motion re-compensation, the echo data could be segmented recursively, accomplishing filtering and down-sampling, outputing the filtered data only containing the information of each sub-image.

In summary, the algorithm mainly includes the following two key parts of recursive segmentation. Part one is to segment the scene recursively, and the other part is to segment the beam recursively and get a set of narrow-beam filtered data. Part one is to serve part two, and the sub-beam recursive segmentation could be stopped as long as each sub-scene is within the limit of the effective focusing scene size.

C. PRECISE FOCUSING VIA STANDARD PFA

As long as the sub-beam is segmented narrow enough to ensure that each sub-scene is within the effective imaging scene radius of the PFA, the classical PFA could be used. 2^{2S} precisely-focused sub-images for 2^{2S} sub-beams will be achieved via PFA, the residual error of the non-center point can be completely negligible and each sub-image achieved via PFA is well focused.

There is one point to be noticed: Each sub-beam has a direction offset from the original scene center, and each sub-beam has its corresponding sub-scene center. Therefore, the LOS direction at aperture center is always changing for different sub-beam data. If PFA still uses the classical LOSPI method, different sub-image would have a different rotation angle from the original coordinate system.

For efficiency, a modified LOSPI method is adopted for polar coordinate interpolation to process the sub-beam data, via which the scene orientation in the output sub-image does not vary with the sub-beam direction, but fixed at the original squint angle. Then all the orientation stabilized sub-images could be mosaicked easily, finally achieving the large image of full scene free of defocus can be obtained.

D. CALCULATION QUANTITATIVE ANALYSIS

The calculation of dot multiplication is small, such as motion re-compensation. FFTs in the recursive segmentation needs some extra calculation but not too much. The biggest operation is the resample of range and azimuth in the final step of standard PFA to each sub-beam data. However, compared to the original data array size of $N \times N$, after the beam-segmenting, there would be 2^{2S} ouput sub-data arrays, each has a small size of $N/2^S \times N/2^S$. Therefore, the final classical PFA processing for each sub-beam data will not increase the computational burden. Therefore, the calculation amount is almost the same as classical PFA.

IV. EXPERIMENTAL RESULTS

A. SIMULATION RESULTS

The highly squinted and high resolution simulation parameters are shown in the Table 1, with a high squint angle of 60°. The distribution map of 9 × 9 simulation points are given in Fig.6 along the (x, y) direction, while the adjacent targets are spaced as 140m along the x-axis and the y-axis. Under the condition of this parameter, the effective scene radius limit of traditional PFA is only about 133m. The imaging area is 1120m × 1120m in square, and the max scene radius should be calculated as 1120 × 1.4/2 (half of the diagonal line), which is almost 800m, which is far beyond the PFA effective imaging scene radius of 133m.

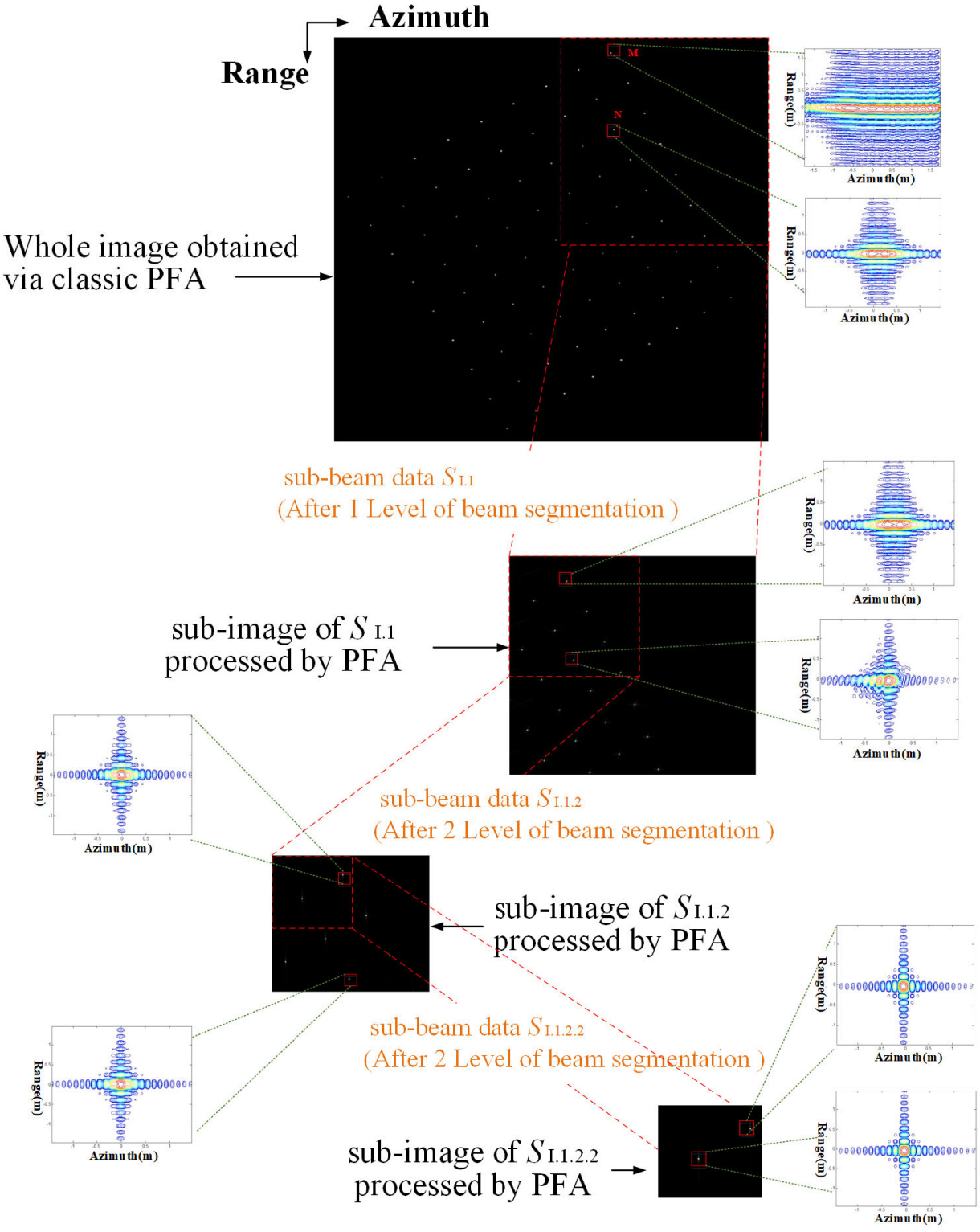

FIGURE 7. Simulated Results of normal PFA method and the proposed PFA method (Including some two dimensional characteristic of some points).

According to the relationship between the PFA effective imaging scene radius and the full scene size, 4 levels of segmentation are required.

The whole image obtained by normal PFA and some certain sub-images obtained during the beam-segmenting process are shown in Fig.7, while the two dimensional target

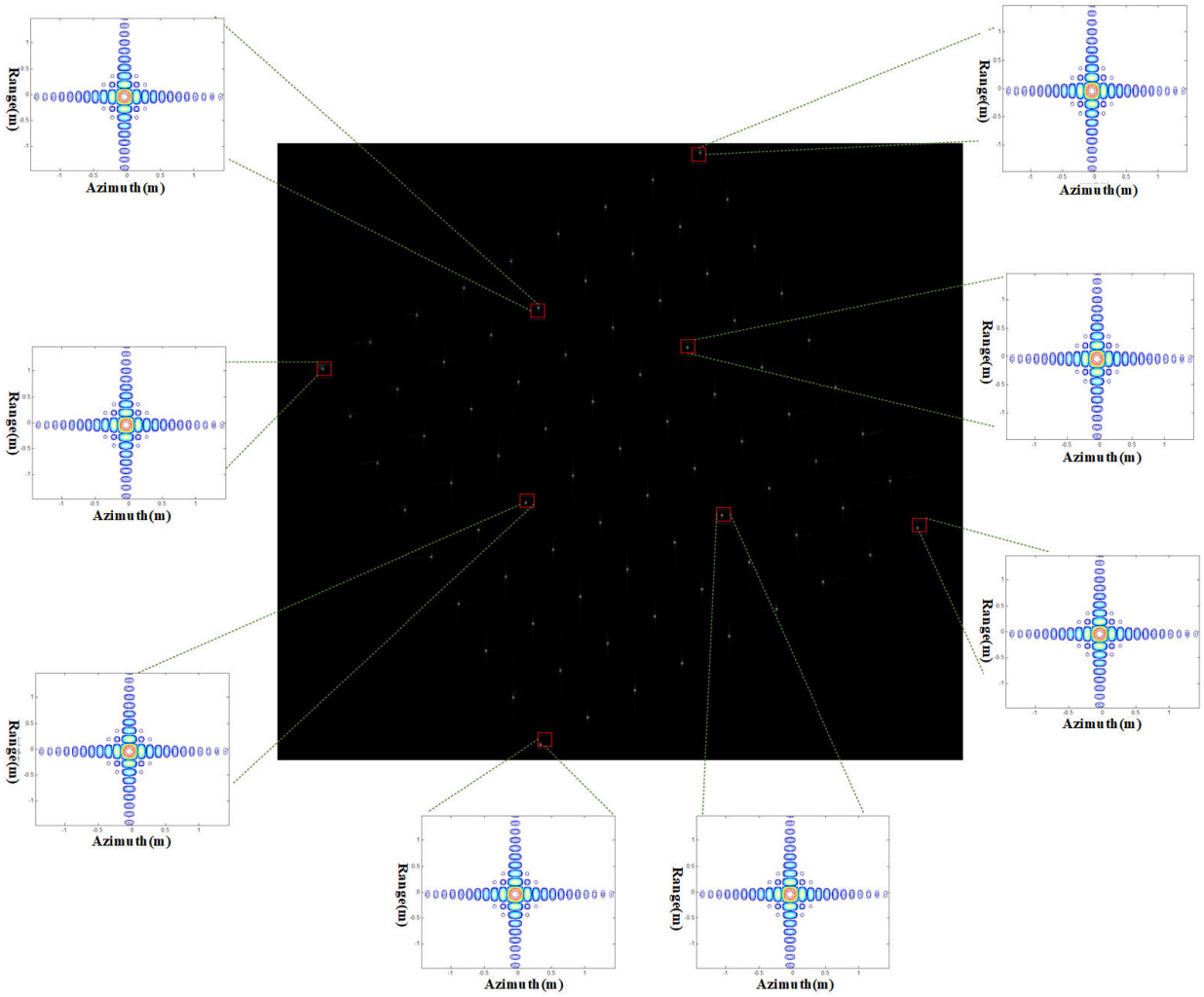

FIGURE 8. Mosaicked whole image via the proposed PFA.

TABLE 1. Simulation parameters.

System parameters	Value	Units
Wavelength	0.03	m
Signal bandwidth	1.2	GHz
Velocity	240	m/s
Height	2000	m
Working range	10000	m
Squint angle	60	°
Resolution	0.15m×0.15	m
PFA size limit r_0	133	m

response characteristic of 2 certain points, one is point M (at the edge of the scene), and the other is point N, is displayed as well.

It can be seen that the whole image processed by normal PFA has obvious geometric distortion, and there is very serious defocus for point M and N obtained by PFA.

If use normal PFA to process sub-beam data S*I.1*, i.e. if the beam-segmenting is stopped after 1-level of segmentation, the sub-image of S*I.1* is shown in Fig.7. It can be seen that the obvious geometric distortion is primarily corrected, and the point target is better focused than the original level. Anyway, the defocus still exists, so only 1-level of segmentation is obviously insufficient. Further segmentation is indispensable.

Until 4-level of beam-segmentation is implemented, each point in the sub-image is focused perfectly. Based on our method, via 4-level of beam-segmentation, 64 precisely focused sub-images are obtained, which could be mosaicked together to get the final well-focused whole-scene big image showed in Fig.8. In Fig.8, it could be seen that each point target is focused perfectly.

B. REAL DATA EXPERIMENTAL RESULTS

We validate the proposed PFA algorithm by real data of a X-band airborne radar with resolution 0.15m and the squint angle 53°. Under the condition of these parameters, the effective scene radius limit of traditional PFA is only about 150m. But the whole scene size is much larger than 2 km×1 km (azimuth × range).

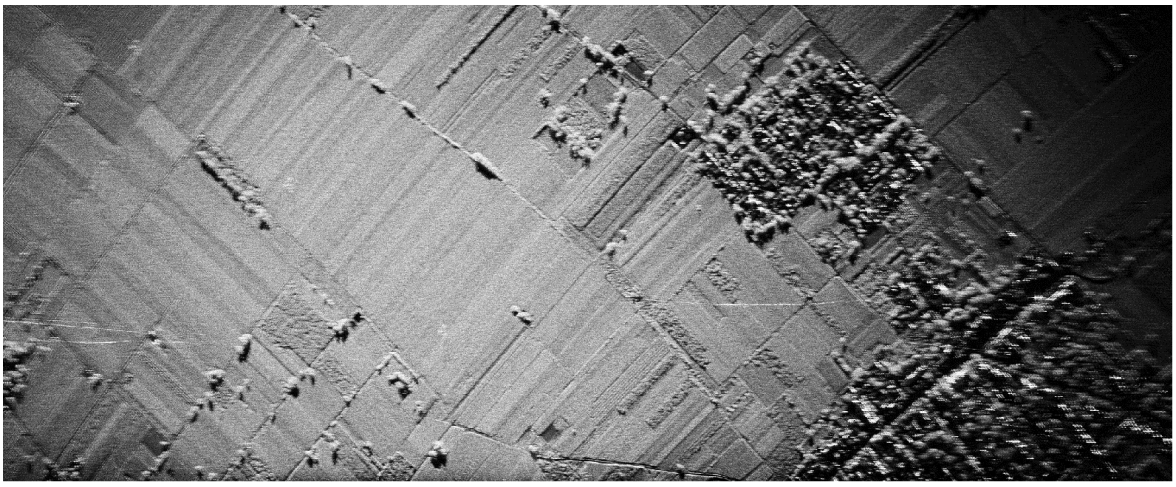

(a)

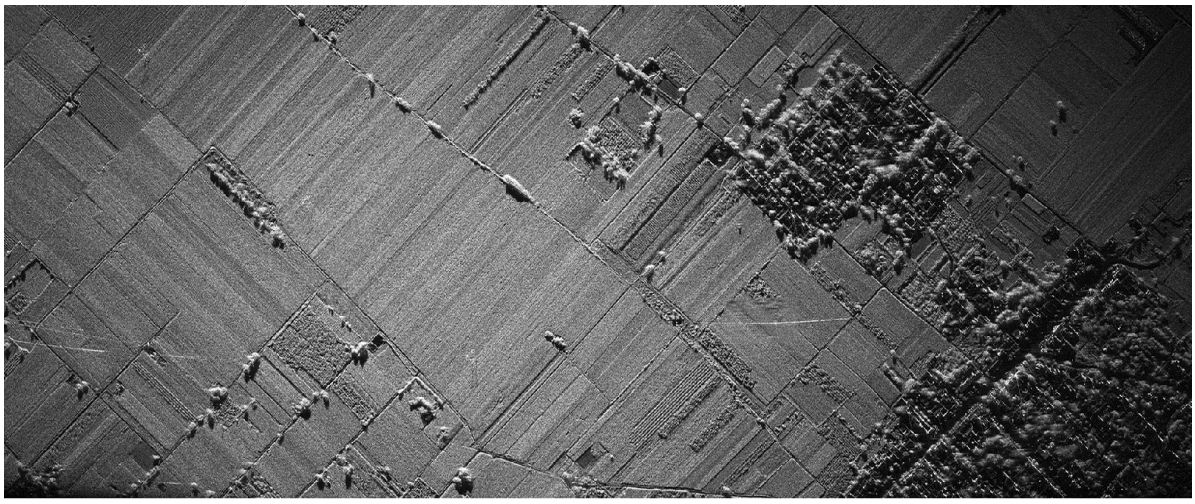

(b)

FIGURE 9. (a) Result of normal PFA method;. (b) Result of the proposed PFA method.

Fig.9 (a) shows the final image obtained by normal PFA. There is serious defocus for the image, since the whole scene size exceeds the PFA effective scene radius limit.

According to the relationship between the PFA effective imaging scene radius and the full scene size, 4 levels of segmentation can control the sub-image within the effective imaging scene radius. Fig.9 (b) shows the final image obtained by the new PFA. It can be seen that all regions are well focused and have no stitching traces. It proves that the proposed method can break the PFA size limit, and it could achieve well-focused wide-swath image.

V. CONCLUSION AND FURTHER DISCUSSION

In this paper, a new quadtree beam-segmenting based PFA is proposed. Actually, this algorithm includes two parts of recursive segmentation. One part is to segment the image recursively, and the other part is to segment the echo data recursively.

This procedure is equivalent to generate multiple narrow sub-beam raw data by filtering the original echo data recursively until each sub-beam is filtered narrow enough for standard PFA. The desired resolution could be retained for each sub-beam, since the synthetic aperture length for each sub-beam is retained changeless, and it is as long as the original aperture which is long enough to get the desired resolution. And the data of each sub-beam is not divided into fragmented sub-apertures, while the new approach utilizes the whole aperture as a total solution, so the resolution is maintained really well.

The simulation and measured data results show that even in the situation of high squint angle, the proposed method can avoid the residual error of each target and achieve precisely-focused wide-swath image.

This divide-and-conquer approach breaks the image size limit in traditional PFA, extensively enlarges the effective focused scene. Since this method is not based on the formula

derivation of residual error, it is not restricted by the derivation order and can theoretically be extended to handle scene arbitrary large, and it has its unique advantage in highly-squinted SAR. Since normal PFA is adapted to any squint angle smaller than 85°, so the presented approach can deal with the squint angle no larger than 85° as well.

REFERENCES

[1] J. Walker, "Range-Doppler imaging of rotating objects," *IEEE Trans. Aerosp. Electron. Syst.*, vol. AES-16, no. 1, pp. 23–52, Jan. 1980.
[2] W. G. Carrara, R. S. Goodman, and R. M. Majewski, *Spotlight Synthetic Aperture Radar: Signal Processing Algorithms*. Norwood, MA, USA: Artech House, 1995.
[3] C. V. Jakowatz, D. E. Wahl, P. H. Eichel, D. C. Ghiglia, and P. A. Thompson, *Spotlight-Mode Synthetic Aperture Radar: A Signal Processing Approach*. Boston, MA, USA: Kluwer, 1996.
[4] T. Zeng, Y. Li, Z. Ding, T. Long, D. Yao, and Y. Sun, "Subaperture approach based on azimuth-dependent range cell migration correction and azimuth focusing parameter equalization for maneuvering high-squint-mode SAR," *IEEE Trans. Geosci. Remote Sens.*, vol. 53, no. 12, pp. 6718–6734, Dec. 2015.
[5] Z. Li, M. Xing, Y. Liang, Y. Gao, J. Chen, Y. Huai, L. Zeng, G.-C. Sun, and Z. Bao, "A frequency-domain imaging algorithm for highly squinted SAR mounted on maneuvering platforms with nonlinear trajectory," *IEEE Trans. Geosci. Remote Sens.*, vol. 54, no. 7, pp. 4023–4038, Jul. 2016.
[6] Z. Li, Y. Liang, M. Xing, Y. Huai, Y. Gao, L. Zeng, and Z. Bao, "An improved range model and omega-K-based imaging algorithm for high-squint SAR with curved trajectory and constant acceleration," *IEEE Geosci. Remote Sens. Lett.*, vol. 13, no. 5, pp. 656–660, May 2016.
[7] P. Wang, W. Liu, J. Chen, M. Niu, and W. Yang, "A high-order imaging algorithm for high-resolution spaceborne SAR based on a modified equivalent squint range model," *IEEE Trans. Geosci. Remote Sens.*, vol. 53, no. 3, pp. 1225–1235, Mar. 2015.
[8] Z. Li, Y. Liang, M. Xing, Y. Huai, L. Zeng, and Z. Bao, "Focusing of highly squinted SAR data with frequency nonlinear chirp scaling," *IEEE Geosci. Remote Sens. Lett.*, vol. 13, no. 1, pp. 23–27, Jan. 2016.
[9] S. Tang, L. Zhang, P. Guo, G. Liu, and G.-C. Sun, "Acceleration model analyses and imaging algorithm for highly squinted airborne spotlight-mode SAR with maneuvers," *IEEE J. Sel. Topics Appl. Earth Observ. Remote Sens.*, vol. 8, no. 3, pp. 1120–1131, Mar. 2015.
[10] Z. Li, M. Xing, W. Xing, Y. Liang, Y. Gao, B. Dai, L. Hu, and Z. Bao, "A modified equivalent range model and wavenumber-domain imaging approach for high-resolution-high-squint SAR with curved trajectory," *IEEE Trans. Geosci. Remote Sens.*, vol. 55, no. 7, pp. 3721–3734, Jul. 2017.
[11] Y. Liang, Y. Huai, J. Ding, H. Wang, and M. Xing, "A modified ω-k algorithm for HS-SAR small-aperture data imaging," *IEEE Trans. Geosci. Remote Sens.*, vol. 54, no. 6, pp. 2450–2462, Jun. 2016.
[12] L. Zeng, Y. Liang, M. Xing, Y. Huai, and Z. Li, "A novel motion compensation approach for airborne spotlight SAR of high-resolution and high-squint mode," *IEEE Geosci. Remote Sens. Lett.*, vol. 13, no. 3, pp. 429–433, Mar. 2016.
[13] S. I. Tsunoda, F. Pace, J. Stence, M. Woodring, W. H. Hensley, A. W. Doerry, and B. C. Walker, "Lynx: A high-resolution synthetic aperture radar," *Proc. SPIE*, vol. 3704, pp. 1–8, Jul. 1999.
[14] N. Xin, L. Wanming, and S. Shijian, "The investigation of high-resolution sliding-spotlight SAR imaging algorithms," (in Chinese), *Electron. Technol. Softw. Eng.*, vol. 4, pp. 71–73, 2016.
[15] J. Yang, G. Sun, J. Chen, L. Mao, and M. Xing, "A subaperture imaging algorithm to highly squinted TOPS SAR based on SPECAN and deramping," in *Proc. Eur. Conf. Synth. Aperture Radar*, Berlin, Germany, 2014, pp. 398–401.
[16] Z. Sun, J. Wu, Z. Li, Y. Huang, and J. Yang, "Highly squint SAR data focusing based on keystone transform and azimuth extended nonlinear chirp scaling," *IEEE Geosci. Remote Sens. Lett.*, vol. 12, no. 1, pp. 145–149, Jan. 2015, doi: 10.1109/LGRS.2014.2329554.
[17] X. Mao, D. Zhu, and Z. Zhu, "Polar format algorithm wavefront curvature compensation under arbitrary radar flight path," *IEEE Geosci. Remote Sens. Lett.*, vol. 9, no. 3, pp. 526–530, May 2012.
[18] M. Soumekh, *Synthetic Aperture Radar Signal Processing With MATLAB Algorithm*. New York, NY, USA: Wiley, 1999, ch. 1.
[19] M. Soumekh, D. A. Nobles, M. C. Wicks, and G. R. J. Genello, "Signal processing of wide bandwidth and wide beamwidth P-3 SAR data," *IEEE Trans. Aerosp. Electron. Syst.*, vol. 37, no. 4, pp. 1122–1141, Oct. 2001.
[20] X. Nie, "Study on ultra-high resolution SAR imaging algorithms," Ph.D. dissertation, Dept. Signal Inf., Nanjing Univ. Aeronaut. Astronaut., Nanjing, China, 2010.
[21] Y. Li, "Study on airborne and missile-borne synthetic aperure radar imaging algorithms based on subaperture processing," Ph.D. dissertation, Dept. Signal Inf., Nanjing Univ. Aeronaut. Astronaut., Nanjing, China, 2005.

XIN NIE was born in Shanxi, China, in December 1983. She received the Ph.D. degree from the Nanjing University of Aeronautics and Astronautics, Nanjing, in 2010.

She is currently a Researcher with the Nanjing Research Institute of Electronics Technology. She has authored or coauthored over 20 articles. Her major research interests include system design, radar imaging, synthetic aperture radar (SAR) processing for high-resolution, and highly-squinted and wide-swath SAR systems.

LONG ZHUANG was born in Jiangsu, China, in 1979. He received the master's degree in signal and information processing from the Nanjing Research Institute of Electronics Technology, Nanjing, China, in 2005, and the Ph.D. degree in signal and information processing from Shanghai Jiaotong University, Shanghai, China, in 2009.

He is currently with the Nanjing Research Institute of Electronics Technology. His major research interests include MIMO radar signal processing and SAR/ISAR imaging.

SHIJIAN SHEN was born in Jiangsu, China, in 1983. He received the master's degree in signal and information processing from the Nanjing Research Institute of Electronics Technology, Nanjing, China, in 2008.

He is currently with the Nanjing Research Institute of Electronics Technology. His major research interests include radar signal processing and target detection.